



LAWRENCE
LIVERMORE
NATIONAL
LABORATORY

The High-betaN Hybrid Scenario for ITER and FNSF Steady-State Missions

F. Turco, C. Holcomb

August 9, 2016

Physics of Plasmas

Disclaimer

This document was prepared as an account of work sponsored by an agency of the United States government. Neither the United States government nor Lawrence Livermore National Security, LLC, nor any of their employees makes any warranty, expressed or implied, or assumes any legal liability or responsibility for the accuracy, completeness, or usefulness of any information, apparatus, product, or process disclosed, or represents that its use would not infringe privately owned rights. Reference herein to any specific commercial product, process, or service by trade name, trademark, manufacturer, or otherwise does not necessarily constitute or imply its endorsement, recommendation, or favoring by the United States government or Lawrence Livermore National Security, LLC. The views and opinions of authors expressed herein do not necessarily state or reflect those of the United States government or Lawrence Livermore National Security, LLC, and shall not be used for advertising or product endorsement purposes.

The High- β_N Hybrid Scenario for ITER and FNSF Steady-State Missions

F. Turco¹, C.C. Petty², T.C. Luce², W. Solomon³, C.T. Holcomb⁴, J.R. Ferron², T.N. Carlstrom²,
M.A. Van Zeeland², W. Heidbrink⁵

¹Columbia University, New York, New York USA

²General Atomics, P.O. Box 85608, San Diego, California 92186-5608 USA

³Princeton Plasma Physics Laboratory, Princeton, New Jersey USA

⁴Lawrence Livermore National Laboratory, Livermore, California USA

⁵University of California, Irvine, Irvine, California USA

Abstract. New experiments on DIII-D have demonstrated the steady-state potential of the hybrid scenario, with 1 MA of plasma current driven fully non-inductively and β_N up to 3.7 sustained for ~ 3 s (~ 1.5 current diffusion time, τ_R , in DIII-D), providing the basis for an attractive option for steady-state operation in ITER and FNSF. Excellent confinement is achieved ($H_{98y2} \sim 1.6$) without performance limiting tearing modes. The hybrid regime overcomes the need for off-axis current drive efficiency, taking advantage of poloidal magnetic flux pumping that is believed to be the result of a saturated 3/2 tearing mode. This allows for efficient current drive close to the axis, without deleterious sawtooth instabilities. In these experiments, the edge surface loop voltage is driven down to zero for $>1 \tau_R$ when the poloidal β is increased above 1.9 at a plasma current of 1.0 MA and the ECH power is increased to 3.2 MW. Stationary operation of hybrid plasmas with all on-axis current drive is sustained at pressures slightly above the ideal no-wall limit, while the calculated ideal with-wall MHD limit is $\beta_N \sim 4-4.5$. Off-axis NBI power has been used to broaden the pressure and current profiles in this scenario, seeking to take advantage of

higher predicted kink stability limits and lower values of the tearing stability index Δ' , as calculated by the DCON and PEST3 codes. Results based on measured profiles predict ideal limits at $\beta_N > 4.5$, 10% higher than the cases with on-axis NBI. A 0-D model, based on the present confinement, β_N and shape values of the DIII-D hybrid scenario, shows that these plasmas are consistent with 100% non-inductive operation for the ITER 9 MA, $Q=5$ mission and the FNSF 6.7 MA scenario. With collisionality and edge safety factor values comparable to those envisioned for ITER and FNSF, the high- β_N hybrid represents an attractive high performance option for the steady-state missions of these devices.

1. INTRODUCTION

The ITER and FNSF steady-state missions require plasmas with long duration and fully non-inductive conditions ($f_{NI}=1$) at fusion gain $Q=5$ and $Q \leq 5$ respectively. Extrapolation to these conditions from the current scenarios requires demonstration discharges in present machines and validation of the models used for the extrapolation. In general, the plasma current (I_p) is composed ~~by~~ of the ohmic current (J_{ohm} , inductive), the bootstrap current, and the non-inductive sources driven by Neutral Beam Injection (NBI), Electron Cyclotron (EC) waves, Ion Cyclotron (IC) waves, etc. The first two components are self-generated, while the other sources are generated externally by some part of the input power. Since the present means for NBI and EC current generation have fairly low efficiency, simultaneously meeting the constraints of high fusion gain and fully-noninductive CD entails the maximization of the bootstrap current fraction. However, a complex non-linear interaction links the bootstrap current J_{bs} , the safety factor (q) and the kinetic profiles (n_e , T_e , T_i , Z_{eff} , etc). The magnitude of the bootstrap current is proportional to the plasma pressure; therefore, operation at high-normalized pressure, β_N

($\beta_N = \beta(\%) \cdot a(m) \cdot B_T(T) / I_p(\text{MA})$, where β is the ratio of the plasma pressure to the magnetic field pressure, a the plasma minor radius, B_T the toroidal magnetic field and I_p the plasma current), is required to maximize the bootstrap current generation. In general, the external current drive efficiencies are proportional to the local electron temperature, and inversely proportional to the density. All these quantities usually peak on-axis, and the external CD sources are most effective where T_e is higher. Therefore, high β_N is not only required to obtain a large enough fraction of bootstrap current (f_{BS}), but it is also a consequence of utilizing heating sources for a large amount of current drive (all the present heating sources also drive the non-inductive current mentioned so far).

In order to achieve fully-noninductive conditions, the sum of the non-inductive sources (external CD and bootstrap) have to align to the total current profile (J) that gives the q profile desired for the scenario. For this to be stationary, these conditions have to be achieved without Ohmic current (which is inherently transient), therefore, the non-inductive sources, in the final desired condition, have to be positioned in a way that substitutes the Ohmic current over the whole radius. This usually requires a significant part of the current to be moved from the center to mid-radius, which has proven challenging and potentially power expensive.

The hybrid scenario, obtained in several machines [1-5], has the attractive characteristic of a self-organized current profile, which derives from a "flux pumping" mechanism transferring part of the central CD to an off-axis position. This is believed to be caused by the presence of a saturated, benign $m=3/n=2$ or $m=4/n=3$ tearing mode, located at $\rho \sim 0.25-0.4$, which only slightly degrades the confinement, without creating a β_N or I_p collapse. For a more detailed discussion of the flux pumping mechanism we refer to [6,7]. For this reason, the issue of aligning the external current sources to the total current does not apply to the hybrid plasmas, which eliminates one of

the challenges faced by the other candidates for steady-state operation. All the non-inductive current can be driven centrally around $\rho \sim 0$, where T_e and T_i are large, and the CD efficiency is highest. Despite all the central current drive, the flux pumping mechanism produces a q profile that remains slightly above 1 for the duration of the discharges. This eliminates the $m=1/n=1$ internal kink mode, and no sawteeth appear even after several current diffusion times.

Throughout the paper we will compare the $q_{min} \sim 1$ hybrid scenario to the higher $q_{min} \geq 1.5$ scenarios, from the perspective of performance and MHD stability. The latter is the more standard high- β_N scenario envisioned for steady-state operation in future machines. It is usually characterised by higher q_{min} ($1.5 < q_{min} < 2.5$), high normalized pressure and wall stabilization [8-10].

The hybrid discharges were designed to have reverse B_T direction with respect to the I_p direction, to take maximum advantage of the off-axis current [11], which places the $B \times \nabla B$ drift direction towards the upper divertor. Both double-null (DN) and lower single-null (SN) discharges were studied. We will mainly report on the DN, biased ~~up~~-downwards and roughly balanced cases. The full power of the co-injected neutral beam system was used, amounting to ~ 11 MW, with an additional ~ 4 MW of counter-injected power, as a first attempt to reduce the external torque. The ECCD power in these plasmas ranges between 2.4-3.2 MW, the injection is tangential with co- I_p driven current, and the deposition location is kept as close as possible to the plasma center ($\rho \sim 0.05-0.25$), in a slightly broad shape to avoid excessive localized peaking of the profiles.

At high β_N , plasmas are usually closer to a stability limit, either resistive or ideal, or both. In high- β_N steady-state hybrids, the $m=2/n=1$ tearing mode appears more readily at high normalized pressure and, despite not causing disruptions, it degrades the confinement significantly, causing

the loss of 20 to 50% of the plasma stored energy. Moreover, this mode perturbs the current profile in a way that is not recoverable with the available current sources. It has been shown [10,12] that the tearing stability of a high β_N plasma is strongly correlated with its proximity to the ideal MHD with-wall limit. The tearing index Δ' shows a sharp increase to very large values when the equilibrium is approaching an ideal limit (figure 20 in reference 10), and under these conditions tearing modes are more susceptible to destabilization. Moreover, when the equilibrium is close to the ideal limit, the equilibrium is extremely sensitive to small perturbations, which may move the ideal limits slightly - in this steep region where Δ' increases rapidly, a small variation of the ideal limit causes large variations in Δ' , and hence in the tearing stability. Since operating at lower β_N is typically not a viable option for steady-state scenarios, which require high f_{BS} , one approach is to modify the equilibrium to increase the ideal limit: pushing the ideal limit to higher β_N values allows us to have a high β_N scenario, while operating in the region where Δ' varies slowly, has reduced values, and so is less sensitive to equilibrium perturbations.

It has been shown [8,10] that the ideal MHD limit increases with broader pressure and current profiles, for high q_{min} equilibria. Given the attractive characteristics of the hybrid scenario, it is crucial to investigate whether this approach can be beneficial also to the hybrid $q_{min} \sim 1$ plasmas. The tilted, off-axis NBI line in DIII-D was designed to provide 4 MW of heating and current drive power deposited at $\rho \sim 0.4$, and was utilized in the 2013-2014 hybrid campaign to broaden the pressure and current profiles of high β_N hybrid plasmas. This means that roughly 35% of the NBI power is deposited at 40% of the minor radius, when one of the NB lines is tilted at the maximum angle. While applying this concept to the hybrid scenario may benefit the MHD

stability, it is also important to verify how much the use of off-axis heating may degrade the confinement of these plasmas.

In the following sections we will present the comparison between on-axis and off-axis heating effects on hybrid confinement and performance (section 2), while in section 3 we will discuss the MHD activity present in moderate to high- β_N hybrid plasmas. The path to fully-noninductive conditions in high- β_N hybrid plasmas will be presented in section 4, and in section 5 we report on the ideal MHD and tearing limits of the scenario. We will present the extrapolation of the present plasmas to the ITER and FNSF relevant scenarios in section 6 and discussion of the particular needs and characteristics of the scenario for burning plasma devices are presented in the last section (7).

2. PERFORMANCE OF HYBRID PLASMAS WITH ON- AND OFF-AXIS NBI

The use of off-axis NBI heating may cause a reduction in confinement and lower β_N levels for a given amount of NBI power, which would impact the bootstrap fraction and hinder the achievement of fully non-inductive conditions. In order to utilize the off-axis NBI system to enhance the MHD stability of the discharges, an assessment of the **potential** change in confinement **potentially** associated with it is needed. An example of hybrid discharges with a slightly lower biased DN shape, off-axis NBI, high $\beta_N=3.66$ and surface loop voltage (V_{loop}) near zero for ~ 2 s is shown in figure 1. The discharges are stable to the 2/1 tearing mode, and their duration is limited by the energy available in the neutral beam system. The NBI power was optimized over 3 repeat shots to achieve the longest duration and maximized power yield on the β_N flattop (2.3 to 4.8 s), which in turn maximizes β_N and minimizes V_{loop} . The current diffusion time τ_R in these plasmas is $\tau_R \sim 1.75$ s, hence the high β_N and zero loop voltage duration of 2.5 s is

equivalent to $\sim 1.4 \times \tau_R$. The density was also optimized to obtain good confinement and to minimize the loop voltage. Lower density shots also yield slightly lower $\beta_N \sim 3.2-3.4$ and slightly higher $V_{loop} \sim 5-10$ mV. For reference, we show the comparison with the more standard high- q_{min} scenario typical time traces in figure 2: for comparable density and q_{05} values, the hybrid discharge (black traces) reaches the same β_N level as the high- q_{min} case (orange traces), while sustaining this β_N for ~ 1 s longer duration. The H_{98y2} and V_{loop} values are also reproduced by the hybrid plasma, while the lower $q_{min} \sim 1$ is shown in the bottom part of the figure.

Since it was observed that higher density yields better confinement, a line averaged density scan was performed, in order to explore higher β_N levels, and investigate (i) at what density the positive effect on confinement stops, and (ii) what β_N level can be achieved. Increasing the density increases β_N , which in turn increases f_{BS} , but this may not be sufficient to counteract the decrease in CD efficiency with increased density. Therefore, the high density, higher β_N shots move away from fully non-inductive conditions, but they are useful to study the MHD stability closer to the ideal with-wall limit. In figure 3 we show the comparison between a $\tilde{n}_e \sim 4 \times 10^{19} \text{ m}^{-3}$ and the $\tilde{n}_e \sim 5 \times 10^{19} \text{ m}^{-3}$ case that yields the highest β_N achieved in DIII-D hybrids so far. The shots plotted in black and green have on-axis NBI, while the one plotted in red is sustained with ~ 4 MW of off-axis NBI. All cases have $P_{NBI} \sim 11$ MW, $P_{ECH} \sim 3.2$ MW with central CD injection at $\rho \sim 0.05-0.25$. It is crucial to note that the plasma with $\sim 36\%$ of off-axis heating reaches exactly the same conditions and the same high β_N as the case with on-axis NBI. This shows that there is no confinement penalty for moving parts of the NBI power away from $\rho=0$, up to 40% of the normalised minor radius. On the other hand, when the density is increased by $\sim 25\%$ from $\tilde{n}_e \sim 4 \times 10^{19} \text{ m}^{-3}$, the plasmas with $\tilde{n}_e \sim 5 \times 10^{19} \text{ m}^{-3}$ reach $\beta_N \sim 4-4.2$, a 10-15% increase from the

$\beta_N \sim 3.66$ value. The H_{98y2} factor increases from ~ 1.55 to ~ 1.75 , when β_N increases up to $\beta_N \sim 4.2$ just before a 2/1 tearing mode starts. This is true for both the on-axis and off-axis NBI cases.

3. MHD ACTIVITY IN HIGH- β_N HYBRIDS

Hybrid discharges with $\beta_N \geq 4$ are limited by MHD modes, while the confinement increases enough to allow for potentially higher β_N values, as suggested by the $\beta_N = 4.2$ points. Before being terminated by the tearing instability, the $\beta_N = 4$ cases have been sustained for ~ 800 ms on the flat-top phase. The beneficial effect of increased density on the confinement saturates at $\tilde{n}_e \sim 5 \times 10^{19} \text{ m}^{-3}$, i.e. the higher density discharges with $\tilde{n}_e \sim 6 \times 10^{19} \text{ m}^{-3}$ reach $\beta_N \sim 4$, without any further improvement. The $m=3/n=2$, $m=4/n=3$ modes are beneficial for the scenario and the deleterious $m=2/n=1$ modes can be avoided up to $\beta_N \sim 3.6$ (the discharges are passively stable in that case). However, bursts of MHD activity are present in several cases at this β_N level, appearing as fishbone-like events with higher frequency with respect to the 2/1 tearing modes ($f_{\text{bursts}} \sim 25\text{-}50 \text{ kHz}$, $f_{2/1} \sim 10\text{-}15 \text{ kHz}$). These modes, shown in figure 4, have a fairly fast growth time, $\tau_{\text{bursts}} \sim 1 \text{ ms}$, compared to the tearing modes, which grow in $\tau_{\text{TM}} \sim 10 \text{ ms}$. The radial field measurements (time derivative) from a magnetic probe array are shown in the two bottom boxes, with a zoom over the recurrent bursts. The burst pattern is similar to a fishbone type mode, with in some cases an abrupt decay of the oscillations (box f). Given the large fraction of fast ions generated by the NBI system and the low $q_{\text{min}} \sim 1$, these modes would be consistent with fast-ion fishbones associated with the 1/1 surface. Nevertheless, the activity level does not decrease at higher density values, which is not consistent with expected fishbone behavior. When this type of activity ceases in the high- β_N flat-top phase, the normalized pressure usually increases, indicating that the confinement was partially degraded during the bursting events.

Another aspect of the MHD activity found in these high power plasmas is the presence of Alfvén Eigenmodes (AEs), which develop at higher frequencies ($f_A \sim 200$ kHz in these $q_{min} \sim 1$ plasmas). The high- β_N hybrids appear to have a low level AE activity, consistent with the standard low- q_{min} plasmas. The amplitude of the AE activity decreases with increasing values of toroidal field, while the use of off-axis NB power does not appear to reduce it. In figure 5 we show an example of the typical density fluctuation spectrogram in the AE frequency range, obtained by evaluating the cross-power of two line-averaged density chords of the CO2 system. The low frequency activity (50-75 kHz) in the higher β_N cases (boxes c and d) represents the previously discussed fishbone-like bursts, while the AE appear at a low level around and above the white dashed line, representing the AE frequency for those plasmas. The higher β_N cases are characterized by higher line averaged density and, of the two cases presented in boxes c and d, the discharge with off-axis NBI (box d) shows a slightly higher AE activity, before the 2/1 tearing mode is triggered (~ 3 s).

4. PRESSURE AND CURRENT DRIVE IN HYBRID PLASMAS WITH ON- AND OFF-AXIS NBI

The concept of broadening the pressure and current profiles to enhance the MHD stability has been applied to higher q_{min} scenarios with some success [8,10] The same amount of off-axis power (~ 4 MW) was used in DIII-D hybrid discharges to evaluate whether (i) the resulting profiles would be in fact broader, given the somewhat fixed central portion of the plasma, and (ii) the ideal and tearing MHD stability would be affected. The fast-ion pressure and density profiles are calculated by means of the NUBEAM code, tuned with an ad-hoc time-varying parameter representing a fast-ion diffusion coefficient so that the calculated stored energy matches the measured plasma stored energy values during the discharges. In figure 6 we

compare the fast-ion pressure profiles of 2 set of discharges which reach $\beta_N \sim 3.6$ (left box) and $\beta_N = 4$ (right box) with and without off-axis power. In the $\beta_N = 3.6$ case, the line averaged density is $\tilde{n}_e \sim 4 \times 10^{19} \text{ m}^{-3}$ and the off-axis injection has a significant effect on the pressure profile (several profiles from the β_N flattop phase of both discharges are plotted to indicate the variability of the results). The fast ion content inside $\rho \sim 0.45$ is significantly reduced in the case of off-axis NBI, and the central fast-ion pressure values are 2.5-3 times higher in the case of the on-axis NBI. In the right box the higher β_N set is shown, where the density is also higher ($\tilde{n}_e \sim 5 \times 10^{19} \text{ m}^{-3}$), and the impact of the off-axis power is less pronounced. For the higher density cases the off-axis fast-ion pressure profiles appear only slightly less peaked, with a factor of ~ 1.6 between the central pressure of the on-axis NBI and the off-axis NBI cases. The fast-ion β_N is $\beta_{fast} \sim 3.5-7.2\%$ for the on-axis NBI cases, while it's slightly lower, $\beta_{fast} \sim 1.9-6.3\%$, for the off-axis cases.

Since the thermal pressure changes **in moving** from on-axis to off-axis NBI are very limited, the fast-ion effects have a small impact on the overall changes in the pressure peaking factor ($f_p = p_{(\rho=0)} / \langle p \rangle$, where the brackets represent the volume averaged pressure) of the database. This is shown in figure 7, where the pressure peaking factors of all the discharges with (red squares) and without (black circles) off-axis NBI are plotted against the achieved β_N , for several time slices on their stationary β_N flattops. **Noting that the zero was suppressed in the plot**, for comparable β_N values, the off-axis power reduces f_p by $\sim 10\%$, although a few outliers are present in the database. It is interesting to note that, in the case of the higher q_{min} scenarios, the achieved β_N values span $\beta_N \sim 3-3.6$, and the pressure peaking factors of those plasmas fall in a lower range, $f_p \sim 2.8-3.3$. Despite having higher pressure peaking factors, which are usually associated with

lower MHD limits [8-10], we will show that the hybrid regime is characterized by ideal and tearing limits comparable to those calculated for the high- q_{min} plasmas (section 5).

The picture for the current profile is more complicated, because of the anomalous current diffusion typical of the hybrid scenario, and the non-linear dependencies between J_{BS} , q and the kinetic profiles introduced in the first section. An example of the non-inductive currents **sources** **of** in an on-axis (full lines) and off-axis case (dashed lines) are presented in figure 8. The off-axis NBI case has much less NBI current (blue) in the centre, but this is compensated for by a significantly larger contribution from the bootstrap current (red), which shows a peak inside $\rho \sim 0.2$, not present in the on-axis profiles. These differences are summarized in figure 9, where we compare the sum of all the non-inductive **sources currents** for the on- and off-axis case, compared to the total current profile as measured by the equilibrium reconstruction based on magnetics, MSE and kinetic profiles data. Evidence of the anomalous current diffusion mechanism is given by the large discrepancy between the central calculated and measured current, indicating clearly that part of the central poloidal flux is being transported outside of $\rho \sim 0.3$. The usual location of the stationary, low amplitude 3/2 mode is given by the green shaded area. A more detailed picture of the typical current density profiles that characterize the β_N flattop phase of these plasmas is in figure 10. Several time slices at $\beta_N \sim 3.66$ and $\beta_N \sim 4$ are reported, in order to give an idea of the variability of the results. This confirms the description given previously, where the off-axis NBI mainly seems to reduce the central peak of the NBI current, while the total current density is more affected by the changes in the bootstrap current (red traces in figure 8). This is the cause of the larger amount of current at $\rho \sim 0.2-0.4$, while the less peaked NBI current profile is the cause of the lower central current density in the off-axis

cases. Some differences seem to appear also in the pedestal region; the pedestal profiles and MSE data are still under investigation, and will be deferred to a future paper.

With the calculated current drive from the NB and EC systems and the self-generated bootstrap current, the total plasma current is completely non-inductively generated when 3 MW of ECCD power are used and the bootstrap fraction reaches $\sim >45\%$ at $q_{95} \sim 5.5-6.5$. The path to fully non-inductive conditions is shown in figure 11, where the measured surface loop voltage at the edge is represented against the values of poloidal β (β_p) for all discharges in the double-null, high q_{95} database. The loop voltage is driven to zero by decreasing the plasma current slightly from 1.1 MA to 1.0 MA and from there by increasing the ECH power by ~ 800 kW, from ~ 2.4 MW to 3.2 MW (equivalent of 2 extra gyrotrons used in the shots). We highlight two outliers in order to point out the hidden variable in the study: all the plasmas in the plot have line averaged densities of $\sim 3.5-3.9 \times 10^{19} \text{ m}^{-3}$, while the high β_p cases with $V_{\text{surf}} \geq 10$ mV have 10% and 30% higher density level, which drives the plasmas away from fully non-inductive conditions. If we isolate the cases with on-axis NBI (black circles), it is interesting to note that the best conditions for non-inductive drive occur for the same I_p, B_T values as for the off-axis cases. This indicates that the V_{loop} vs I_p, B_T landscape is not affected by the use of off-axis heating, so either on-axis and off-axis NBI can be chosen in the future, depending on the specific goals of the experiment, while maintaining the non-inductive conditions.

5. IDEAL AND TEARING MHD LIMITS OF HYBRID PLASMAS WITH ON- AND OFF-AXIS NBI

Together, the pressure and the current profile characteristics affect the ideal MHD and the tearing stability limits of a plasma. The DCON code [13] is used to calculate the ideal no-wall and with-wall β_N limits, and it includes a smoothed model of the DIII-D vessel wall coordinates.

The ideal limits are evaluated by progressively increasing the pressure of experimental equilibria in a self-similar fashion, keeping the q profile and the total plasma current fixed for all iterations. A sensitivity study showed that the choice of keeping the current profile fixed, instead of the q profile, leads to a difference in the calculated limits of $\sim 5\text{-}10\%$ in β_N . In figure 12, we report the results of the DCON calculations for a series of hybrid discharges with $\beta_N \sim 3.3\text{-}4.2$, characterizing the ideal with-wall limit evolution during the β_N ramp and flat-top phases. The blue traces show the β_N time evolution of several hybrid plasmas with similar characteristics, spanning the range of achieved $\beta_N \sim 3.3\text{-}4.1$. The black circles represent the β_N limits for the plasmas with on-axis NBI, while the red squares are the limits for the corresponding off-axis plasmas. The variability in the results is represented by the various symbols for each time slice. Each discharge evolution has been analyzed by making different assumptions for the plasma density profile fits (e.g. reflectometry or Thomson measurements for the core and vice versa for the pedestal region), and by the presence of constraints on the value of the q profile at $\rho=0$ (e.g. no constraints, $q_0=1.03$, $q_0=1.06$).

Taking into account these variations in the equilibrium reconstructions, the ideal β_N limit without a wall (figure 12-b) ranges between $\beta_N \sim 2.5$ and $\beta_N \sim 4$, while the with-wall limit (figure 12-a) is $\beta_N \sim 3.5\text{-}4.8$, where most of the β_N flat-top points are clustered around $\beta_N=4.5$. When all the ideal with-wall limits for the hybrid database are brought together, it is clear that the limited decrease in the pressure peaking factor with off-axis NBI leads to a rather small increase in the ideal limits of the off-axis cases with respect to the plasmas with on-axis NBI. This is shown in figure 13, where the calculated ideal with-wall limits are plotted against the achieved β_N values for all the time slices on the β_N flat-top of the hybrid database. For comparable achieved β_N , the

increase in the ideal limits for the off-axis cases, **on average**, is $\sim 10\%$, which brings the values from $\beta_{lim}=4.1-4.7$ to $\beta_{lim}=4.4-5.2$ for the best cases.

For comparison, **we report the achieved and projected ideal limit range for the higher q_{min} scenario (orange shaded area in figure 13). This scenario, usually operated at $q_{min}\sim 1.5-2.5$, is characterized by ideal with wall limits of $\beta_{lim}\sim 3.5-4.2$, for achieved β_N levels of $\beta_N < 3.6$. Projected limits for further optimized higher q_{min} plasmas reach $\beta_{lim}\sim 5$, as calculated in [14]. This indicates that the presently achieved β_N limits of the hybrid scenario are comparable with the limits projected for the higher q_{min} AT plasmas.**

The tearing stability of the equilibria can also be calculated, using the PEST3 code [15]. The tearing index Δ' represents the energy available for the plasma to tear, and it is useful to evaluate the first order effects on the tearing stability evolution. The values of the calculated Δ' are very sensitive to small details of the current and pressure profiles in these high- β_N equilibria, so only the relative trends are meaningful for this kind of study. In figure 14, we show the Δ' evolution for a series of stable hybrid discharges, calculated for the same equilibrium reconstruction variations described for the ideal MHD limit study. **Each square symbol reports the Δ' value associated with the plasma equilibrium for each time slice, also shown in the β_N and I_i traces on the same plot. In some cases, various Δ' values are reported, as calculated for slightly different equilibrium reconstructions of the same shot and time slice, to show the variability of the results in the database.** Two discharges at higher β_N , where a large $m=2/n=1$ tearing mode sets in at $t\sim 3$ s, are represented in figure 15, with the respective Δ' evolution. The Δ' values are evaluated for the $m=2/n=1$ surface, considering the $m=2$, $m=3$ and $m=4$ surfaces to be resonant and coupled. Despite the variability in Δ' values across the various discharges, the results suggest that the two

unstable discharges are associated with increasing trends for the tearing index Δ' leading up to the mode. On the other hand, 3 of the 4 stable cases show a decreasing trend in Δ' all the way to the end of the shot, while the fourth case appears to have little variation in the Δ' values over the β_N flattop; the trend stays horizontal until the end of the shot. This is an indication that the higher β_N discharges are evolving towards a more unstable state, which is consistent with the triggering of the large 2/1 tearing mode in the experiment.

6. PROJECTING THE STEADY-STATE HYBRID SCENARIO TO ITER AND FNSF

The extrapolation of a scenario to future devices can be done with a 0-D model [18], to determine the feasibility of the hybrid scenario in burning plasma devices. The input parameters, such as the geometry, the density, B_T , I_p , are scaled up to the values of the desired machine. In this study we compare a ρ^* scaling based on the present scenario density and a specified Greenwald fraction (f_{GW}) to obtain the input plasma density. The output parameters are determined self-consistently in the model, which yields the H_{98y2} factor, the temperature and the fusion, alpha and current drive power (P_{fus} , P_α and P_{CD} respectively). The profiles shapes are specified, based on the experiment profiles parameters, and the β_N and q_{95} values are kept fixed at those in the present scenario. A realistic central current drive efficiency is evaluated from the ITER physics basis [19], as a function of the plasma density, temperature and major radius, $\gamma_{CD} = I_{CD} n_{19} R / P_{CD} = 2.5 \times 10^{19} \text{ A/m}^2 \text{W}$ at $T_e = 20 \text{ keV}$. We assume that 50% of the total plasma current is constituted by the bootstrap current, a fraction consistent with the values calculated for the present hybrid scenario. This allows us to calculate the current drive power needed to sustain the external current source. The input operating parameters used for the steady-state hybrid scenario are reported in table 1, for a deuterium plasma in DIII-D and D-T plasmas in ITER and FNSF.

To study the feasibility of the hybrid scenario in ITER we choose a lower density, lower β_N , LSN hybrid discharge, which is compatible with RMP ELM mitigation and has $f_{BS} \sim 50\%$ with $\beta_N \sim 2.84$ and line averaged density $\tilde{n}_e \sim 3.2 \times 10^{19} \text{ m}^{-3}$. This lower β_N type of hybrid has been proven to reach fully non-inductive conditions, with a lower confinement quality ($H_{98y2} = 1.3$). For the FNSF scaling, the DN hybrid scenario with $\beta_N \sim 3.66$, $\tilde{n}_e \sim 4.1 \times 10^{19} \text{ m}^{-3}$ is used.

Using the ρ^* scaling for the density $\tilde{n}_e = B^{4/3} a^{-1/3}$, the projected ITER and FNSF densities are calculated, and the new temperature and stored energy W are scaled based on the DIII-D β_N and β_T values with the following scaling formulas:

$$\beta_T^{thermal} = \beta_T^X \beta_T^{D3D}, \text{ where we project } \beta_T^X = \frac{I_p}{aB}$$

$$T_0 = \frac{\beta_T^{thermal} B_T^2 (1 + SN + ST)}{4.027 \cdot 10^{-3} n_0 (1 + f_{imp} + fuel_{frac} f_{He})}$$

$$\beta_T^\alpha = 0.29 \beta_T^{thermal} (fuel_{frac}/2)^2 (T_0/10 - 0.37)$$

$$\beta_T = \beta_T^{thermal} + \beta_T^\alpha$$

$$W = \frac{3 \beta_T^{thermal} V B^2}{1.6 \pi}$$

$$P_{HEATING} = \left(\frac{W}{0.0282 I_p^{0.831} B_T^{0.069} \tilde{n}_e^{0.488} R^{2.107} \epsilon^{-0.3} H_{mass}^{0.14} \kappa^{0.75}} \right)^{1/0.45}$$

$$P_{BREM} = \frac{5.34 \cdot 10^{-3} V Z (n_0/10)^2 \sqrt{T_0}}{1 + 2SN + 0.5ST}$$

$$P_{FUSION} = 7.043 \cdot 10^{15} \cdot 2V (fuel_{frac} \cdot n_0/10)^2 T_0^2 \cdot fus_{int}$$

$$fus_{int} = 1.64 \cdot 10^{-19} (-0.455383 + 0.218998 T_0 - 0.0089152 T_0^2 + 0.000103742 T_0^3)$$

$$P_\alpha = P_{FUSION} / 5$$

$$\tau_E = \frac{W}{P_{HEATING} - P_{BREM}}$$

$$\tau_{98y2} = (P_{HEATING} - P_{BREM})^{-0.69} \cdot 0.144 I_p^{0.93} B_T^{0.15} (\tilde{n}_e/10)^{0.41} R^{1.97} \kappa^{0.78} \epsilon^{-0.58} H_{mass}^{0.19}$$

$$H_{98y2} = \frac{\tau_E}{\tau_{98y2}}$$

$$Q_{fus} = \frac{P_{FUSION}}{P_{HEATING} + P_{BREM} - P_\alpha}$$

where $SN=n_0/\tilde{n}_e$, $ST=0.75$ are profile shape factors describing the degree of peaking of the measured density and temperature profiles, $f_{imp}=0.01$, $Z_{imp}=10$, $f_{He}=0.059$ for the ITER case and $f_{He}=0.018$ for the FNSF case, $fuel_{frac}=1-2f_{He}f_{imp}Z_{imp}$.

Taking into account the estimated bremsstrahlung radiation (P_{BREM}), these parameters allow to estimate the auxiliary power needed to sustain the chosen β_N value ($P_{HEATING}$), the power needed to drive the external current in excess of $I_p f_{BS}$ (P_{CD}), the fusion and alpha powers (P_{FUSION} and P_α), and the resulting H_{98y2} factor and fusion energy gain Q_{fus} . In table 2 the results of this scaling are reported for a DN FNSF scenario and a LSN ITER scenario. Taking into account the

alpha power, which drives minimal current, the calculated auxiliary power is sufficient to drive 100% of the plasma current. If the Greenwald fraction is increased slightly, to match the present $f_{GW}=0.46$, it is easy to reach $Q_{fus}=3.1$, with the same H_{98y2} factor and still enough auxiliary heating power to obtain fully non-inductive operation (table 3). It is noteworthy that the present DN SS-hybrid scenario obtained in DIII-D has basically achieved the required values of β_N , Q_{fus} , H_{98y2} and Greenwald fraction for the FNSF scenario.

For the ITER $Q=5$ scenario, a solution with $Q_{fus}>5$ can be obtained with the lower β_N SN hybrid case, but the density is very high ($f_{GW}=1.17$) and both the fusion and current drive powers exceed the ITER objectives and capabilities. However, it is possible to design a more modest steady-state scenario, with lower, but relevant, fusion gain ($Q_{fus}=4.4$) and lower density, by imposing $f_{GW}=0.9$ and calculating the new temperature needed to keep β_N constant. Under these more favourable conditions, the current drive efficiency is higher, which reduces P_{CD} to a more manageable level, while the resulting H_{98y2} is still $H_{98y2}=1.4$. In this case the auxiliary heating power, if used to drive current, is sufficient to reach 100% non-inductive conditions.

It is important to note that these projections have been performed based on model hybrid discharges without counter-NBI injection, i.e. all co- I_p current and torque injection. This results in a high external torque of ~ 8.8 Nm. It is expected that ITER may have much lower external input torque values, due to its larger volume; therefore, it will be necessary to extend the all-co-NBI steady-state hybrid scenario to low torque conditions. Work has started to extend the scenario to lower values of external torque by utilizing the neutral beam line injecting current and torque in the direction opposite to the plasma current. This method provides 4 MW of extra NB power, and ~ 3.2 Nm torque in the counter- I_p direction. By adding the counter- I_p NBI source to an existing high- β_N hybrid discharge, the external torque is reduced by $\sim 35\%$, from ~ 8.8 Nm

to ~ 5.6 Nm, while the total injected power reaches ~ 19 MW. However, the counter-NBI system is detrimental to the discharge confinement time τ_E , which decreases by $\sim 18\%$, and the confinement factor H_{98y2} , which decreases by 22% . With the additional 35% of auxiliary power, the discharge reaches the same β_N flattop value as the co-injected case, hence, the confinement decreases.

From the perspective of the scaling work presented in this section, the effects of this choice are limited: as shown in the equations above, the projected stored energy W is based on the measured β_T , which is the same for the all-co-NBI discharges and the corresponding counter-NBI cases. This is used to evaluate P_{HEATING} , and therefore τ_E , τ_{98y2} and H_{98y2} . The temperature and density profiles appear similar for the co-NBI cases and the counter-NBI injection case available, and this is consistent with the fact that the higher power, lower torque case reaches the same β_N as the co-injected cases. Since the heating power for the scaled scenario is not projected from the presently used input power, but instead from the presently achieved W and β_T , the projected H_{98y2} and Q_{fus} values do not change significantly for the lower torque cases. However, this is a consequence of the type of scaling method, and since a lower confinement factor and a lower confinement time is observed in the present counter-injected discharges, it is reasonable to expect that this may project to the ITER and FNSF scenarios, which could potentially require more auxiliary power (P_{HEATING} in this study) to reach the projected W . Therefore, operating the hybrid scenario at low torque may entail obtaining lower confinement factor and Q values than those extrapolated from the present high-torque plasmas.

7. DISCUSSION AND CONCLUSIONS

Steady-state hybrid plasmas have been obtained in DIII-D with a DN plasma shape, $\beta_N \geq 3.5$ and zero surface loop voltage for $\sim 1.5 \tau_R$, being limited only by the available NB system energy. These plasmas are characterized by a flat q profile, at $q_{95} = 5.5-6.5$, and are generally stable to deleterious $2/1$ tearing modes. Although the central current is theoretically overdriven by the use of efficient NB and EC current drive close to the axis, an anomalous current diffusion mechanism, believed to stem from a small saturated $3/2$ tearing mode, maintains q_{min} above 1, avoiding sawtooth instabilities. The discharges exceed the ideal no-wall β_N limit and reach 80-90% of the calculated with-wall limit. The confinement quality of these plasmas is excellent ($H_{98y2} = 1.6$) and appears to increase with density, up to line averaged densities of $\tilde{n}_e \sim 5 \times 10^{19} \text{ m}^{-3}$. The highest β_N cases, obtained with $\tilde{n}_e \sim 5 \times 10^{19} \text{ m}^{-3}$, exceed $\beta_N = 4$ and reach 80-90% of the calculated ideal wall β_N limit. These cases are sustained for ~ 800 ms in the β_N flattop, before a growing $2/1$ mode is triggered. The TAE activity level of these discharges is consistent with the usual TAE amplitudes characterizing low q_{min} plasmas. The use of $\sim 35\%$ of off-axis NB heating increases the calculated ideal limits by $\sim 10\%$, without any confinement penalty.

On the other hand, adding 4 MW of counter-injected NBI power decreases the confinement time and the confinement factor by $\sim 20\%$, and does not lead to higher β_N values. **The cause of this apparent loss of confinement associate with counter- I_p NBI injection is still under investigation for several DIII-D scenarios.** However, this is the first step toward operating the hybrid scenario at lower injected torque values, which is among the requirements for future burning plasma devices. Furthermore, in order for the hybrid scenario to be considered compatible with future machine operation, it is necessary to extend it in several directions, besides low torque operation, such as an ELM suppressed regime, integration with a radiating

divertor, and electron heating schemes. Encouraging results have been obtained in the former, with a lower β_N steady-state version of the hybrid scenario. In these lower pressure hybrids an n=3 RMP technique has successfully suppressed ELMs at $\beta_N=2.4$, and mitigated them at $\beta_N=2.9$. This has been achieved in a LSN plasma shape and at lower density ($\tilde{n}_e \sim 3 \times 10^{19} \text{ m}^{-3}$). Both the DN and the LSN shaped cases lead to fusion gain values compatible with steady-state operation in ITER and FNSF. A 0-D model, based on the present confinement, β_N and shape values of the DIII-D hybrid scenario, shows that these plasmas are consistent with 100% non-inductive operation for the ITER 9 MA, Q=5 mission and the FNSF 6.7 MA scenario.

It is interesting to note that, in the case of these future devices, a fundamental difference will be the presence of the α -heating power, which increases with β_N , and drives minimal current. In the present machines, where the auxiliary power also drives part of the plasma current, the operating point where $f_{NI}=1$ occurs in virtually all cases with a bootstrap fraction that does not exceed 60%, including for the standard higher q_{min} scenarios [8-10,14]. An exception may be the case of plasmas with a strong internal temperature or density gradient, such as an ITB, which will increase the bootstrap fraction for the given β_N level. Under these conditions f_{BS} may reach 60-70% and the external current drive needed for $f_{NI}=1$ will be reduced. In the case of a burning plasma device, the β_N level needed to obtain the desired output power will be sustained in part by the α -heating, which limits the amount of external power capable of driving the plasma current. This is where the more efficient central current drive, which can be used in the hybrid scenario without overdriving the center of the plasma current density profile, is likely to be a very attractive feature. The solution for $f_{NI}=1$ can be achieved with lower β_N values than those needed for $f_{NI}=1$ in a higher- q_{min} scenario, which entail lower f_{BS} values, since the CD efficiency is higher for the central hybrid injection. This makes up for the lower bootstrap current, and for the

presence of the α -heating, which supplies part of the auxiliary power available to sustain the chosen β_N value. The scaling study presented in section 7 confirms this scenario.

Nevertheless, more work is necessary to extend the steady-state hybrid scenario to operating parameters required for ITER and FNSF. Besides the progress made for the low torque and ELM suppression direction, a radiating divertor solution needs to be explored, and prove to be compatible with the high core performance of these plasmas. The next steps also involve increasing the electron heating power to reach $T_e/T_i \sim 1$, which will also go in the direction of reducing the externally injected torque.

Finally, the mechanism that allows for a flat q profile without sawteeth, despite the theoretical current overdrive in the plasma center, is not yet completely understood, and no theory has been put forward to explain it in detail. This is an important point that needs to be addressed, in order to be able to scale this anomalous current diffusion effect to future machines, and prove that the $q_{min} \sim 1$ hybrid conditions can indeed be reproduced in burning plasma devices.

ACKNOWLEDGEMENTS

This material is based upon work supported by the U.S. Department of Energy, Office of Science, Office of Fusion Energy Sciences, using the DIII-D National Fusion Facility, a DOE Office of Science user facility, under Awards DE-FG02-04ER54761, DE-FC02-04ER54698, DE-AC52-07NA27344, SC-G903402, and DE-AC02-09CH11466. DIII-D data shown in this paper can be obtained in digital format by following the links at https://fusion.gat.com/global/D3D_DMP.

REFERENCES

- [1] T.C. Luce, C.D. Challis, S. Ide, E. Joffrin, Y. Kamada, P.A. Politzer, J. Schweinzer, A.C.C. Sips, J. Stober, G. Giruzzi, C.E. Kessel, M. Murakami, Y.-S. Na, J.M. Park, A.R. Polevoi, R.V. Budny, J. Citrin, J. Garcia, N. Hayashi, J. Hobirk, B.F. Hudson, F. Imbeaux, A. Isayama, D.C. McDonald, T. Nakano, N. Oyama, V.V. Parail, T.W. Petrie, C.C. Petty, T. Suzuki, M.R. Wade, the ITPA Integrated Operation Scenario Topical Group Members, the ASDEX-Upgrade Team, the DIII-D Team, JET EFDA Contributors¹³ and the JT-60U Team, 2014 *Nucl. Fusion* **54** 013015
- [2] Sips A.C.C. et al 2002 *Plasma Phys. Control. Fusion* 44 B69.
- [3] Joffrin E. Et al 2005 *Nucl. Fusion* 45 626.
- [4] Isayama A. Et al 2003 *Nucl. Fusion* 43 1272.
- [5] Luce T.C. et al 2001 *Nucl. Fusion* 41 1585.
- [6] Wade M.R. et al 2005 *Nucl. Fusion* **45** 407.
- [7] Petty C.C. et al 2009 *Phys. Rev. Lett.* **102** 045005.
- [8] A.D. Turnbull, T.S. Taylor, et al., Synergism Between Cross-Section and Profile Shaping in Optimization of Tokamak Equilibria with Negative Central Shear,” *Nucl. Fusion* 38, 1467 (1998).
- [9] A.D. Turnbull PRL 1995.
- [10] F. Turco, C.T. Holcomb , J.R. Ferron , T.C. Luce , P.A. Politzer , J.M. Park, A.E. White, D.P. Brennan, A.D. Turnbull, J.M. Hanson , M. Okabayashi , and Y. In, *Phys. Plasmas* **19**, 122506 (2012).
- [11] J.M. Park, M. Murakami, C.C. Petty, W.W. Heidbrink, M.A. Van Zeeland, D.C. Pace, R. Prater, J.R. Ferron, T.H. Osborne, C.T. Holcomb, G.J. Jackson, T.W. Petrie, B.A. Grierson, C.J. Murphy and T. Suzuki, IAEA conference paper.

- [12] D.P. Brennanb, A.D. Turnbull, M.S. Chu, R.J. La Haye, L.L. Lao, and T.H. Osborne, S.A. Galkin, *Phys. Plasmas* **14**, 056108 2007.
- [13] A.H. Glasser and M.S. Chance, *Bull. Am. Phys. Soc.* **42**, (1997) 1848.
- [14] J.R. Ferron, et al *Phys. Plasmas* **20**, (2013) 092504.
- [15] A. Pletzer, A. Bondeson, and R. L. Dewar, *J. Comput. Phys.* 115, 530 (1994).
- [16] T.E. Evans et al *Nature Physics* **2**, June (2006).
- [17] T.E. Evans et al *Nucl. Fusion* **48** (2008) 024002
- [18] V.S. Chan, *FST* **57** (2010) 66
- [19] ITER Physics Basis Editors et al *Nucl. Fusion* **39** (1999) 2137.

LIST OF FIGURE CAPTIONS

Figure 1 Time evolution for β_N (a), H_{98y2} (b), NBI and ECH power (c), line averaged density (d) and surface loop voltage (e) for 3 hybrid discharges with off-axis NBI.

Figure 2 Time evolution for β_N (a), density (b), H_{98y2} (c), NBI and ECH power (d), surface loop voltage (e) and minimum q (f) for a hybrid discharge (black) and a standard AT discharge with higher q_{\min} (orange).

Figure 3 Time evolution for β_N (a), density (b), H_{98y2} (c), NBI and ECH power (d) and perturbed $n=1$ field (e) for 3 hybrid discharges with on-axis NBI (black and green traces) and off-axis NBI (red traces).

Figure 4 Time evolution of β_N (a), continuous $n=1$ mode signal (b), time derivative of the radial field at the wall (c and d), and a zoom over the same traces (e and f) for two off-axis NBI hybrid discharges with $\beta_N=3.7$ (stable, black trace) and $\beta_N=4$ (unstable to a large $n=1$ rotating tearing mode at ~ 3.1 s, red traces). The green shaded area indicates the times with no large tearing modes and the presence of the fast bursting activity.

Figure 5 Spectrogram of the high frequency MHD activity amplitude based on the density fluctuations measured by the CO2 system. Discharges with on-axis beams on the left column, with off-axis NBI on the right, $\beta_N=3.66$ on the top row, $\beta_N=4$ on the bottom row.

Figure 6 Fast-ion pressure profiles for on-axis (black) and off-axis NBI discharges (red), for β_N flattop of 3.6 (left box) and $\beta_N=4$ (right box).

Figure 7 Pressure peaking factor obtained on the β_N flattop of 6 hybrid discharges plotted against the corresponding β_N values. On-axis NBI cases in black, off axis in red.

Figure 8 Calculated EC (green), NBI (blue), bootstrap (red) current density profiles for an on-axis (full lines) and an off-axis NBI (dashed lines) fully-noninductive hybrid discharges.

Figure 9 Calculated plasma current density profile (red) and measured current density (black) for an on axis (full lines) and an off-axis NBI discharge (dashed lines). The radial localization of the $m=3/n=2$ saturated tearing mode is represented by the green shaded area.

Figure 10 Total current density profile (top traces) and NBI current density profiles (bottom traces) comparing on-axis (black) and off-axis NBI cases (red). All time slices are on the β_N flattop.

Figure 11 Surface loop voltage represented against poloidal beta for all the shots in the SS-hybrid database. The blue circles represent the 1.1 MA cases, the green squares the 1.0 MA cases with 4 gyrotrons, the red triangles the 1.0 MA and 6 gyrotrons. The black circles isolate the on-axis NBI cases.

Figure 12 Measured β_N traces (continuous blue lines) and calculated ideal with-wall (a) and no-wall limits (b) for 6 hybrid discharges with on-axis (black circles) and off-axis NBI (red squares).

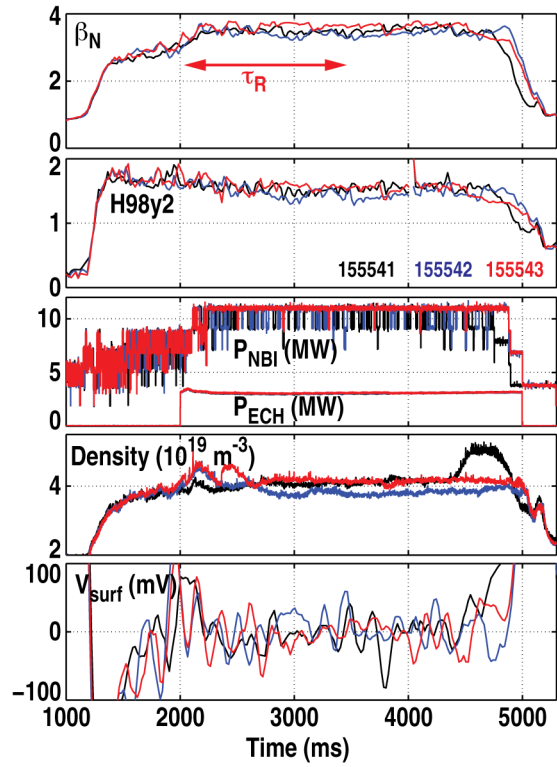
Figure 13 Survey of with-wall β_N limit for 6 discharges in the SS-hybrid database, represented against the achieved β_N values. All points are on the β_N flattop. The red squares are the off-axis NBI cases, the black circles are the on-axis cases. The orange and red shaded areas represent the present with-wall limits for the standard higher q_{\min} scenario and the projected limits for an optimized version of the high q_{\min} scenario.

Figure 14 Evolution of the calculated Δ' values for several equilibria leading up to and on the β_N flattop of 4 hybrid discharges that remain stable until the end. The β_N and li traces are also plotted for reference, and the shaded areas highlight the Δ' trends in time over the high- β_N phase.

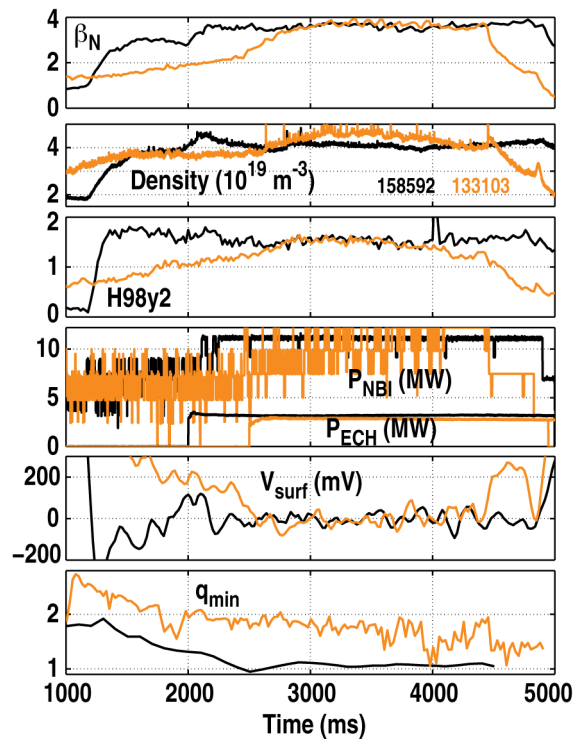
Figure 15 Evolution of the calculated Δ' values for several equilibria leading up to and on the β_N flattop of 2 hybrid discharges that develop a 2/1 tearing mode at $n=3$ s. The β_N and li traces are

also plotted for reference, and the shaded areas highlight the Δ' trends in time over the high- β_N phase.

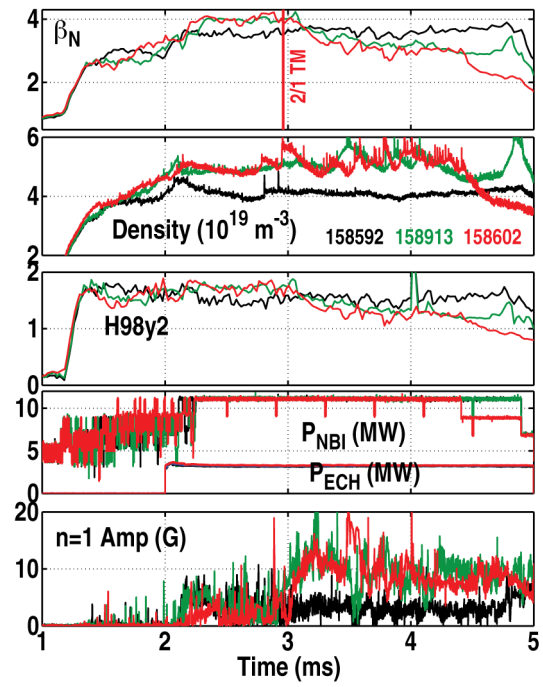
LIST OF FIGURES



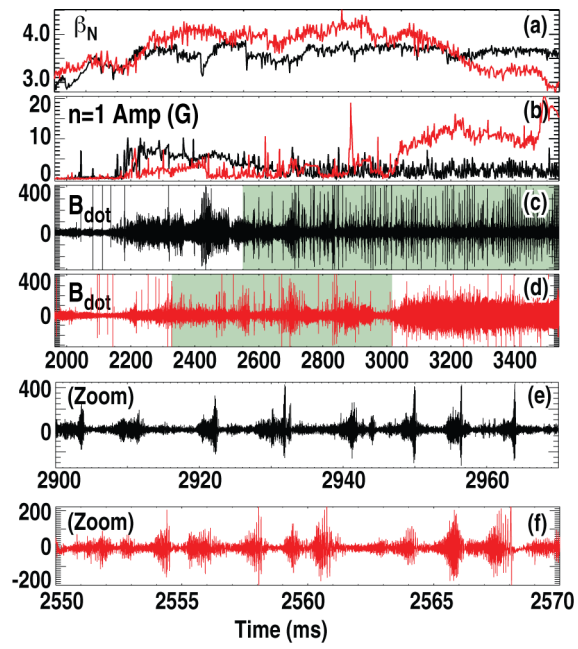
T. Turco Fig. 1



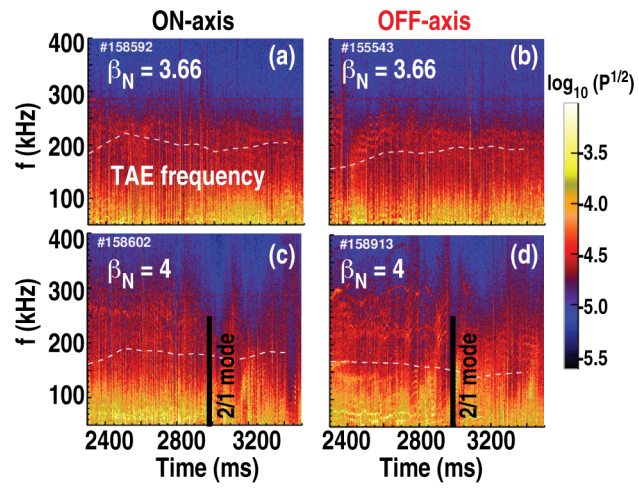
F.Turco Fig. 2



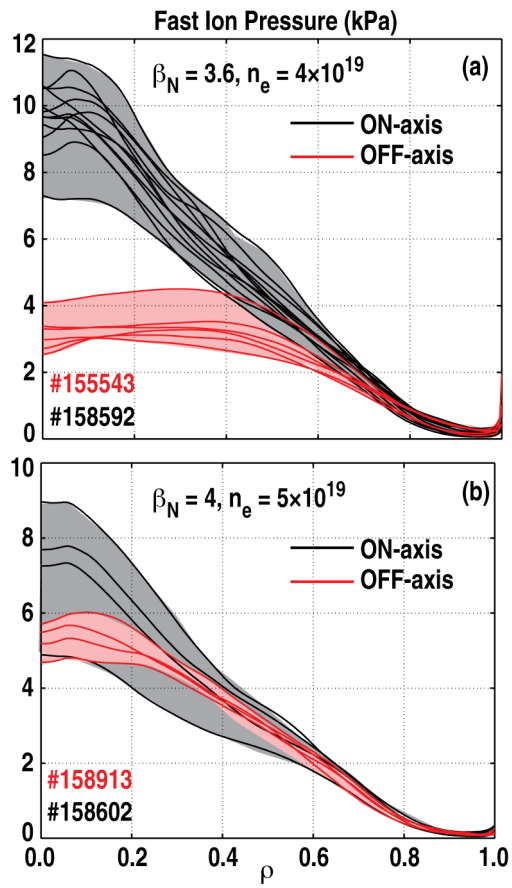
F.Turco Fig. 3



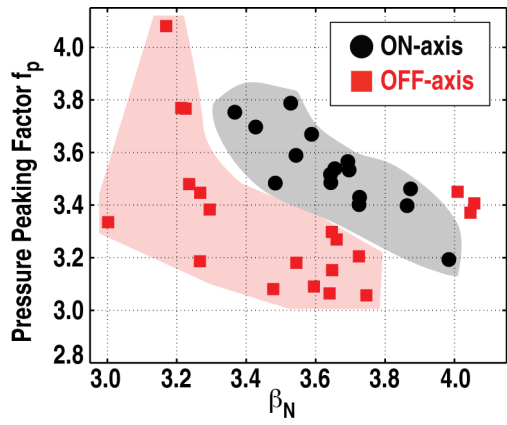
F. Turco Fig. 4



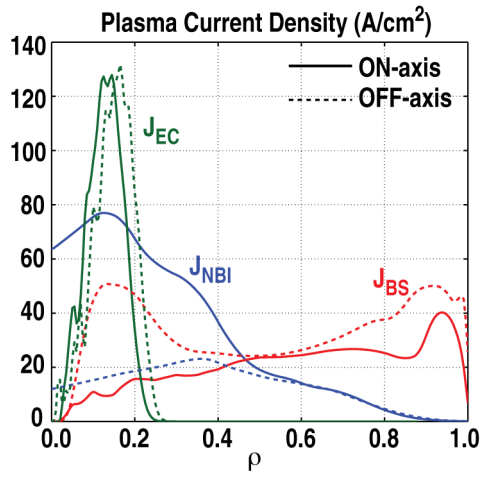
F. Turco Fig. 5



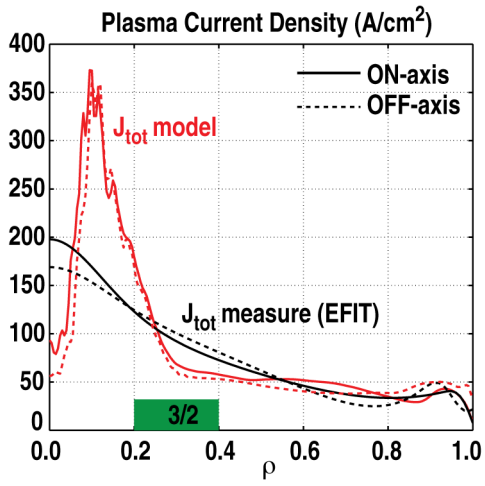
F. Turco Fig. 6



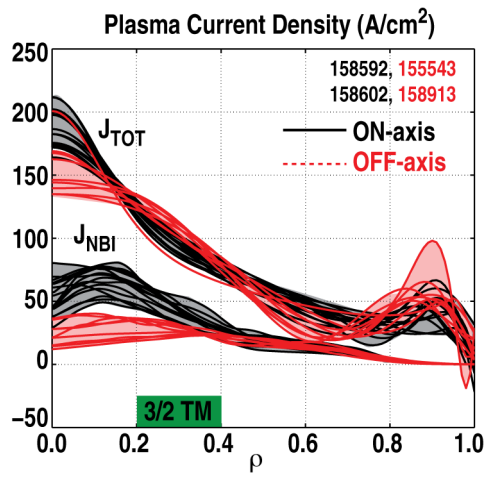
F. Turco Fig. 7



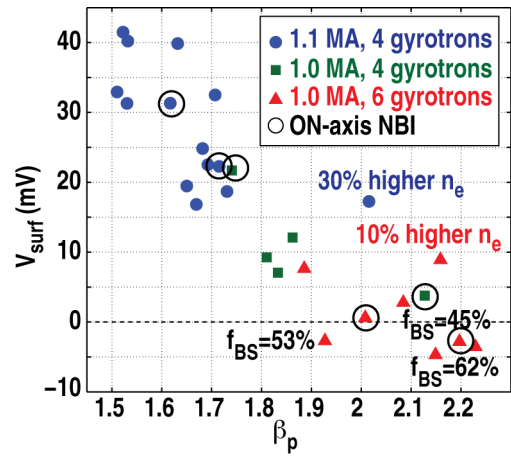
F. Turco Fig. 8



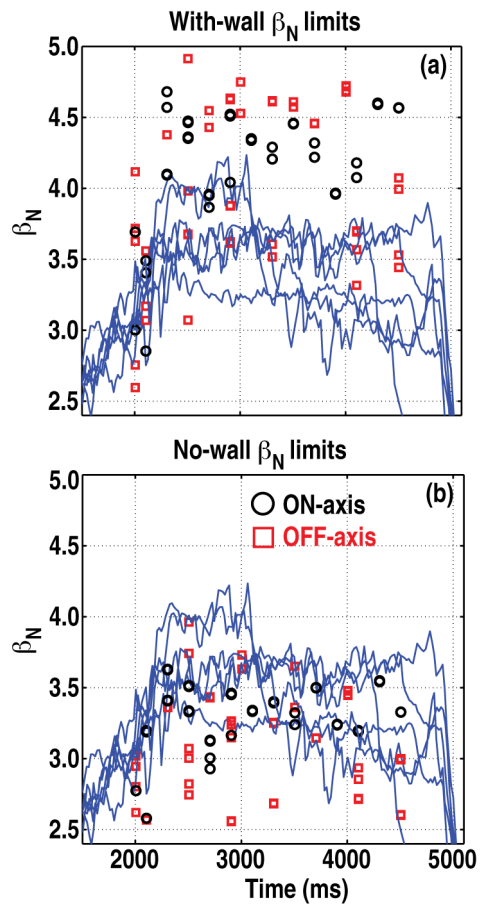
F. Turco Fig. 9



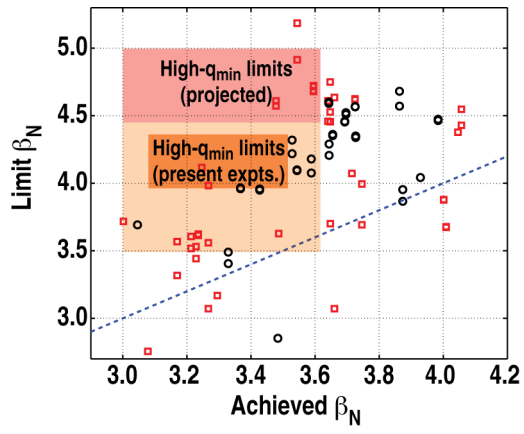
F.Turco Fig. 10



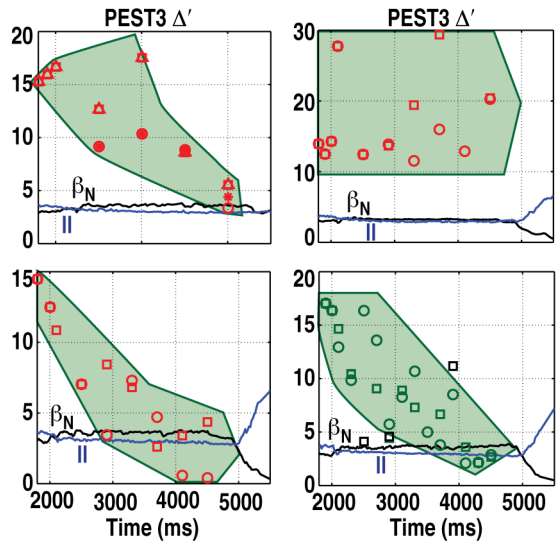
F. Turco Fig. 11



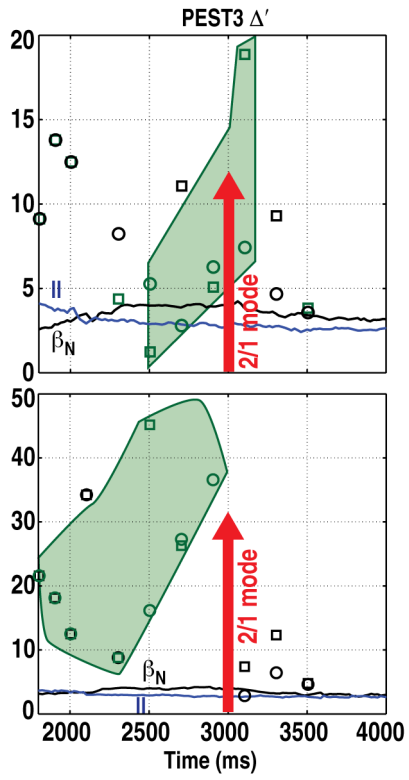
F. Turco Fig. 12



F. Turco Fig. 13



F. Turco Fig. 14



F. Turco Fig. 15